

Associated charmonium-bottomonium production in single boson e^+e^- annihilation

I. N. Belov,^{1,2,*} A. V. Berezhnoy,^{1,†} and E. A. Leshchenko^{2,‡}

¹*SINP MSU, Moscow, Russia*

²*Physics department of MSU, Moscow, Russia*

The production cross sections of $J/\psi \eta_b$, $\Upsilon \eta_c$ pairs in single boson e^+e^- annihilation have been studied in a wide range of energies, which will be achieved at future e^+e^- colliders. The main contributions to the production processes are taken into account, including the one loop QCD contribution.

I. INTRODUCTION

Despite its long history, the heavy quark physics continues to attract the attention of both theorists and experimentalists. Recently, due to the LHC experiments, the BELLE-II experiment and the BES-III experiment almost every year is marked by a discovery in this area. One of the hot topics of research is the quarkonium pair production. It is worth to remind here the intrigue related to the observation of $J/\psi \eta_c$ pair in the e^+e^- annihilation: the theoretical predictions [1] underestimated the real yield measured at BELLE and BaBar [2, 3] by the order of magnitude. This stimulated numerous studies [4], as a result of which the fair agreement with the data has been achieved. The previous year gave researchers a new sensation: the LHCb Collaboration observed the structure in the $J/\psi J/\psi$ spectrum at large statistics [5]. This circumstance led to a real explosion of interest to this topic.

Looking to the future, we study the processes of the paired quarkonium production which can not be observed at the existing experiments due to low interaction energy, namely, the production of $J/\psi \eta_b$ pairs and $\Upsilon \eta_c$ pairs in the e^+e^- annihilation. These processes can be investigated in the framework of several discussed projects: ILC, FCC, and the muon collider. At ILC and FCC, studies are planned at the energies of the order of Z_0 -boson's mass: the

* ilia.belov@cern.ch

† Alexander.Berezhnoy@cern.ch

‡ leshchenko.ea17@physics.msu.ru

energy range announced for FCC is $\sqrt{s} = 90 \div 400$ GeV [6] and $\sqrt{s} = 250$ GeV is proposed for ILC [7]. In the project of muon collider, it is planned to implement the $\mu^+\mu^-$ collisions at energies from 3 TeV to 14 TeV [8], which are beyond the energy range studied in this work.

It is worth to note that the decays of Z_0 -boson to the charmonium and the bottomonium may be of some interest for the experiments at LHC, see [9].

In our previous studies we already have investigated the paired B_c production [10], as well as the $J/\psi J/\psi$ and the $J/\psi \eta_c$ pair production around the Z_0 pole within the NLO approximation [11]. We have found that for these processes the loop corrections essentially contribute to the cross section values. This result is in agreement with the studies of other research groups investigated the paired quarkonium production in the e^+e^- annihilation¹. Both cases of $J/\psi \eta_b$ and $\Upsilon \eta_c$ production are special, because the tree level diagrams with the single gluon exchange can not contribute to the production of $c\bar{c}$ and $b\bar{b}$ pairs in the color singlet states, and therefore the lowest order QCD contribution to these processes contains loops. This one-loop contribution is of the order of $\mathcal{O}(\alpha_{em}^2 \alpha_s^4)$, that is why it makes sense to investigate it with the purely electromagnetic $J/\psi \eta_b$ and $\Upsilon \eta_c$ production which is of the order of $\mathcal{O}(\alpha_{em}^4)$, because $\alpha_s^2 \sim \alpha_{em}$.

It is worth to mention that the one loop QCD diagrams do not contribute to the production of $J/\psi \Upsilon$ -pair in single boson e^+e^- -annihilation. In leading order such a process goes through the electroweak Z_0 boson decay only. As we planned the current work as a continuation of our previous studies on the one loop QCD corrections, in a sense, this process is slightly out of our interest. However, we keep it in our consideration for comparison with $J/\psi \eta_b$ and $\Upsilon \eta_c$ production. Thus, following processes are considered in this study:

$$\left\{ \begin{array}{l} e^+e^- \xrightarrow{\gamma^*, Z_0^*} J/\psi \eta_b, \\ e^+e^- \xrightarrow{\gamma^*, Z_0^*} \Upsilon \eta_c, \\ e^+e^- \xrightarrow{Z_0^*} J/\psi \Upsilon. \end{array} \right. \quad (1)$$

II. CALCULATION TECHNIQUE

The production of the pair of charmonium and bottomonium in single boson annihilation is constrained by several selection rules, which are discussed below.

¹ See also [12], where the photonic production of paired B_c was studied up to NLO.

The production of the J/ψ Υ pairs is not allowed in the photon exchange, as well as it does not go through the vector part of Z_0 vertex due to the charge parity conservation. The J/ψ Υ pairs are produced through the interaction with the axial part of Z_0 vertex only.

As concerned the η_b η_c pair production, it goes neither through the photon exchange, nor through the Z_0 -boson exchange: the photon decay to the η_b η_c pair is forbidden due to the charge parity conservation, and the Z_0 decay to the η_b η_c pair is forbidden due to the combined CP parity conservation.

At the same time the vector-pseudoscalar (VP) pairs: J/ψ η_b and Υ η_c are produced through the exchange of both the photon and the Z_0 -boson.

These selection rules were reproduced directly in our calculations.

As we already pointed out in the introduction the tree level diagrams with the single gluon exchange do not contribute to the discussed processes, and the lowest order QCD contribution to such processes contains loops. This one-loop QCD contribution is of the order of $\mathcal{O}(\alpha_{ew}^2 \alpha_s^4)$ and therefore it could be comparable with the pure electroweak tree level contribution, which is of the order of $\mathcal{O}(\alpha_{ew}^4) \sim \mathcal{O}(\alpha_{ew}^2 \alpha_s^4)$. Thus, when studying these processes, one should take into account the electroweak contribution (EW) of the order of $\mathcal{O}(\alpha_{ew}^2 \alpha_s^4)$, the one loop QCD contribution of the order of $\mathcal{O}(\alpha_{ew}^2 \alpha_s^4)$, and the interference between them of the order of $\mathcal{O}(\alpha_{ew}^3 \alpha_s^2)$:

$$|\mathcal{A}|^2 = |\mathcal{A}^{EW}|^2 + 2Re(\mathcal{A}^{EW} \mathcal{A}^{QCD*}) + |\mathcal{A}^{QCD}|^2. \quad (2)$$

For the more detailed study of the processes we consider the amplitudes with different intermediate bosons separately:

$$\begin{aligned} |\mathcal{A}|^2 = & |\mathcal{A}_\gamma^{EW}|^2 + |\mathcal{A}_Z^{EW}|^2 + 2Re(\mathcal{A}_\gamma^{EW} \mathcal{A}_Z^{EW*}) + \\ & + 2Re(\mathcal{A}_\gamma^{EW} \mathcal{A}_\gamma^{QCD*}) + 2Re(\mathcal{A}_Z^{EW} \mathcal{A}_Z^{QCD*}) + 2Re(\mathcal{A}_\gamma^{EW} \mathcal{A}_Z^{QCD*}) + 2Re(\mathcal{A}_Z^{EW} \mathcal{A}_\gamma^{QCD*}) + \\ & + |\mathcal{A}_\gamma^{QCD}|^2 + |\mathcal{A}_Z^{QCD}|^2 + 2Re(\mathcal{A}_\gamma^{QCD} \mathcal{A}_Z^{QCD*}). \quad (3) \end{aligned}$$

The production of double heavy quarkonia is described in the framework of nonrelativistic QCD (NRQCD). This formalism allows to factor out the perturbative degrees of freedom and therefore separate the production mechanism into hard and soft subprocesses, using the hierarchy of scales for the quarkonia, which is $m_q \gg m_q v$, $m_q v^2$, Λ_{QCD} , where m_q is the heavy quark mass and v is the velocity of heavy quark in the quarkonium. The hard subprocess corresponds

to the perturbative production of $q\bar{q}$ -pair, while the soft subprocess corresponds to the fusion of quarks into the bound state.

To calculate the matrix elements for the studied processes, we start from the matrix element for $e^+e^- \rightarrow c(p_c)\bar{c}(p_{\bar{c}})b(p_b)\bar{b}(p_{\bar{b}})$ with heavy quarks and antiquarks on their mass shells: $p_c^2 = p_{\bar{c}}^2 = m_c^2$ and $p_b^2 = p_{\bar{b}}^2 = m_b^2$. As we put $v = 0$ before the projection onto the bound states, the momentum P of charmonium and the momentum Q of bottomonium are related with the heavy quark momenta as follows:

$$J/\psi, \eta_c \begin{cases} p_c = P/2 \\ p_{\bar{c}} = P/2 \end{cases} \quad \Upsilon, \eta_b \begin{cases} p_b = Q/2 \\ p_{\bar{b}} = Q/2 \end{cases} \quad (4)$$

To form the bound states we replace the spinor products $v(p_{\bar{q}})\bar{u}(p_q)$ by the appropriate covariant projectors for color-singlet spin-singlet and spin-triplet states:

$$\Pi_{J/\psi}(P, m_c) = \frac{\not{P} - 2m_c}{2\sqrt{2}m_c} \not{\epsilon}^{J/\psi} \otimes \frac{\mathbf{1}}{\sqrt{N_c}}, \quad \Pi_{\eta_c}(P, m_c) = \frac{\not{P} - 2m_c}{2\sqrt{2}m_c} \gamma^5 \otimes \frac{\mathbf{1}}{\sqrt{N_c}}, \quad (5)$$

$$\Pi_{\Upsilon}(Q, m_b) = \frac{\not{Q} - 2m_b}{2\sqrt{2}m_b} \not{\epsilon}^{\Upsilon} \otimes \frac{\mathbf{1}}{\sqrt{N_c}}, \quad \Pi_{\eta_b}(Q, m_b) = \frac{\not{Q} - 2m_b}{2\sqrt{2}m_b} \gamma^5 \otimes \frac{\mathbf{1}}{\sqrt{N_c}}, \quad (6)$$

where $\epsilon^{J/\psi}$ and ϵ^{Υ} are the polarizations of the J/ψ and Υ mesons, satisfying the following constraints: $\epsilon^{J/\psi} \cdot \epsilon^{J/\psi*} = -1$, $\epsilon^{J/\psi} \cdot P = 0$, $\epsilon^{\Upsilon} \cdot \epsilon^{\Upsilon*} = -1$ and $\epsilon^{\Upsilon} \cdot Q = 0$.

These operators close the fermion lines into traces and factor out the bound states. The examples of diagrams contributing to the process $e^+e^- \rightarrow J/\psi \eta_b$ are shown in Figure 1.

The factorized matrix elements have the following form:

$$\mathcal{A}(e^+e^- \rightarrow J/\psi \eta_b) = \frac{\langle O_{J/\psi} \rangle^{1/2} \langle O_{\eta_b} \rangle^{1/2}}{N_c} \mathcal{M}_{J/\psi \eta_b}^{\mu} \epsilon_{\mu}^{J/\psi}, \quad (7)$$

$$\mathcal{A}(e^+e^- \rightarrow \Upsilon \eta_c) = \frac{\langle O_{\Upsilon} \rangle^{1/2} \langle O_{\eta_c} \rangle^{1/2}}{N_c} \mathcal{M}_{\Upsilon \eta_c}^{\mu} \epsilon_{\mu}^{\Upsilon}, \quad (8)$$

$$\mathcal{A}(e^+e^- \rightarrow J/\psi \Upsilon) = \frac{\langle O_{J/\psi} \rangle^{1/2} \langle O_{\Upsilon} \rangle^{1/2}}{N_c} \mathcal{M}_{J/\psi \Upsilon}^{\mu\nu} \epsilon_{\mu}^{J/\psi} \epsilon_{\nu}^{\Upsilon}, \quad (9)$$

where $\mathcal{M}_{J/\psi \eta_b}^{\mu}$, $\mathcal{M}_{\Upsilon \eta_c}^{\mu}$, and $\mathcal{M}_{J/\psi \Upsilon}^{\mu\nu}$ are hard production amplitudes of two quark-antiquark pairs projected onto the quark-antiquark states with zero relative velocities and the appropriate quantum numbers by projectors (5) and (6). The NRQCD matrix elements $\langle O_{\Upsilon} \rangle$, $\langle O_{J/\psi} \rangle$, $\langle O_{\eta_b} \rangle$ and $\langle O_{\eta_c} \rangle$ are vacuum-saturated analogs of the NRQCD matrix elements $\langle O(^3S_1) \rangle$ and $\langle O(^1S_0) \rangle$

for annihilation decays defined in [13]. The numerical values of these matrix elements can be estimated from the experimental data on decays [1, 14, 15], or adopted from the potential models, such as [16], using the relation $\langle O \rangle \approx \frac{N_c}{2\pi} |R(0)|^2$, where $R(0)$ is the quarkonium wave function at origin (see Table A.I of Appendix).

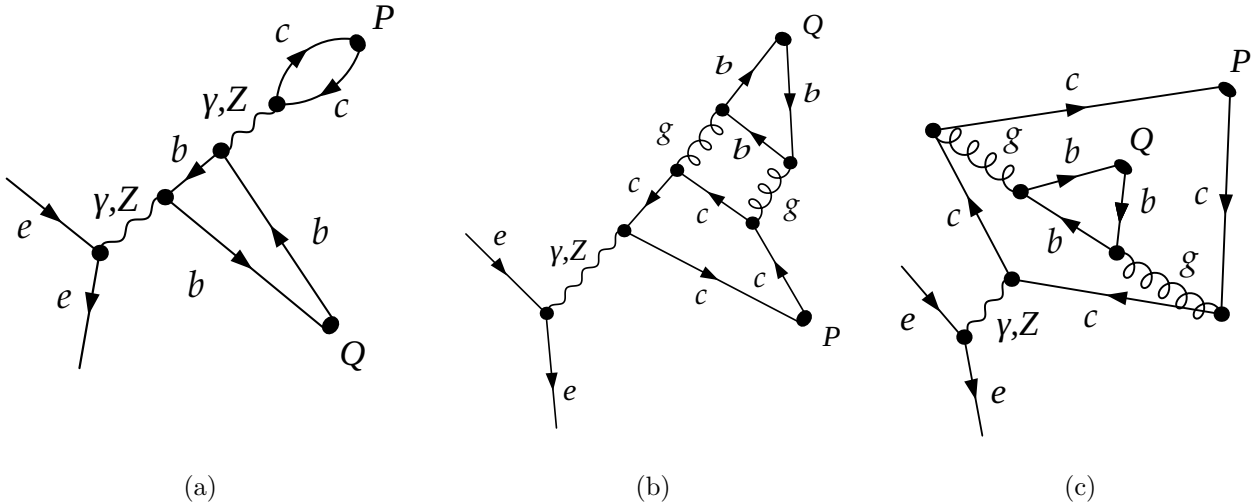


Figure 1. The diagram examples contributing to the $e^+e^- \rightarrow J/\psi \eta_b$ process: (a) – electroweak contribution; (b) and (c) – QCD one loop contribution.

III. WORKFLOW

The diagrams and the corresponding analytic expressions are generated with the `FeynArts`-package [17] in Wolfram Mathematica. The electroweak contribution to the production amplitudes is determined by the tree diagrams of type (a) shown in Figure 1, whereas the one-loop diagrams of type (b) and (c) contribute to the QCD amplitudes.

We obtain 4 nonzero electroweak and 6 nonzero QCD diagrams for each subprocesses $e^+e^- \xrightarrow{\gamma^*} J/\psi \eta_b$, $e^+e^- \xrightarrow{Z^*} J/\psi \eta_b$, $e^+e^- \xrightarrow{\gamma^*} \Upsilon \eta_c$ and $e^+e^- \xrightarrow{Z^*} \Upsilon \eta_c$. The associative production of two vector states J/ψ and Υ is described only by the tree electroweak diagrams of type (a). These results, as well as the explicitly obtained zero contribution to the process of $\eta_b \eta_c$ production, are in exact agreement with the earlier discussed selection rules. This agreement serves as an additional check of our calculations.

To calculate the tree level amplitudes we use only `FeynArts` [17] and `FeynCalc` [18] packages

in `Wolfram Mathematica`, while the estimation of the one loop amplitudes requires a more complicated toolchain: `FeynArts` \rightarrow `FeynCalc(TIDL)` \rightarrow `Apart` [19] \rightarrow `FIRE` [20] \rightarrow `X` [21].

All necessary algebraic calculations with Dirac and colour matrices, including the trace evaluation, are organised within the `FeynCalc` package. At the next step the Passarino-Veltman reduction is carried out using the TIDL library implemented in `FeynCalc`. The `Apart` function does the extra simplification by partial fractioning for IR-divergent integrals. The `FIRE` package provides the complete reduction of the integrals obtained in the previous stages to master integrals. This package implements several strategies for IBP reduction mostly based on the Laporta algorithm [22]. The master integrals are then evaluated by substitution of their analytical expressions with the help of `X`-package.

The conventional dimensional regularization (CDR) scheme with D -dimensional loop and external momenta is used to evaluate the QCD amplitudes. Each QCD amplitude for the separate loop diagram carries a singular term of the order of $\mathcal{O}(1/\varepsilon)$. These terms cancel out after summing over the set of QCD amplitudes, as expected.

It is known that γ^5 is poorly defined in D -dimensions. In the current study the so-called naive interpretation of γ^5 was used: γ^5 anticommutes with all other matrices and therefore disappears in traces with an even number of γ^5 . In traces with an odd number of γ^5 the remaining γ^5 is moved to the right and replaced by

$$\gamma^5 = \frac{-i}{24} \varepsilon_{\alpha\beta\sigma\rho} \gamma^\alpha \gamma^\beta \gamma^\sigma \gamma^\rho. \quad (10)$$

Since $\varepsilon_{\alpha\beta\sigma\rho}$ is contracted after the regularization procedure, we can safely treat it as 4-dimensional.

IV. ANALYTICAL FORM OF THE AMPLITUDES

The relative simplicity of the considered processes makes it possible to provide the analytical expressions for the amplitudes right in the paper.

The electroweak amplitudes of the processes $e^+e^- \rightarrow J/\psi \eta_b$ and $e^+e^- \rightarrow \Upsilon \eta_c$ can be written as follows:

$$\begin{aligned} \mathcal{A}_{EW} (e^+ e^- \rightarrow J/\psi \eta_b) &= \frac{\langle O_{J/\psi} \rangle^{1/2} \langle O_{\eta_b} \rangle^{1/2}}{N_c} \times \\ &\times \frac{-e^4 e_b e_c}{2N_c m_c \sqrt{m_b m_c} (s + 4m_c^2 - 4m_b^2)} \left(b_\gamma J_\mu + b_Z \tilde{J}_\mu \right) \epsilon_\nu^{J/\psi} P_\rho Q_\sigma \varepsilon^{\mu\nu\rho\sigma}. \end{aligned} \quad (11)$$

$$\begin{aligned} \mathcal{A}_{EW} (e^+ e^- \rightarrow \Upsilon \eta_c) &= \frac{\langle O_\Upsilon \rangle^{1/2} \langle O_{\eta_c} \rangle^{1/2}}{N_c} \times \\ &\times \frac{e^4 e_b e_c}{2N_c m_b \sqrt{m_b m_c} (s + 4m_b^2 - 4m_c^2)} \left(c_\gamma J_\mu + c_Z \tilde{J}_\mu \right) \epsilon_\nu^\Upsilon P_\rho Q_\sigma \varepsilon^{\mu\nu\rho\sigma}, \end{aligned} \quad (12)$$

where $e_c = 2/3$ and $e_b = -1/3$ are the quark charges, J_μ and \tilde{J} are the parts of electroweak current which describe the e^+e^- annihilation to the virtual photon and to the virtual Z_0 boson correspondingly ($J_\mu = -i \bar{e} \gamma_\mu e$, $\tilde{J}_\mu = -i \bar{e} \Gamma_\mu^{Z_0} e$), and

$$c_\gamma = \frac{4e_c}{s}, \quad c_Z = \left(\frac{4e_c \sin^2 \theta_w - 1}{\cos \theta_w \sin \theta_w} \right) \frac{1}{s - M_Z^2 + i\Gamma M_Z}, \quad (13)$$

$$b_\gamma = \frac{4e_b}{s}, \quad b_Z = \left(\frac{4e_b \sin^2 \theta_w + 1}{\cos \theta_w \sin \theta_w} \right) \frac{1}{s - M_Z^2 + i\Gamma M_Z}. \quad (14)$$

Such a simple structure of amplitudes (11) and (12) is explained by the fact that only the vector, e. i. the photon-like part of $Z_0 q \bar{q}$ vertex contributes to the boson decays $Z_0^* \rightarrow J/\psi \eta_b$ and $Z_0^* \rightarrow \Upsilon \eta_c$.

It is worth to mention that in the $e^+e^- \rightarrow J/\psi \eta_b$ and $e^+e^- \rightarrow \Upsilon \eta_c$ processes the virtual photon that transforms into the vector meson ($\gamma^* \rightarrow J/\psi$ or $\gamma^* \rightarrow \Upsilon$, see Figure 1(a)) can be complemented by Z_0 boson. Formally, this way we acquire the contributions of the same form as (11) and (12). However ones are extremely suppressed by the Z_0 boson propagator as factors $\left(\frac{m_c^2}{M_Z^2 - 4m_c^2} \right)$ and $\left(\frac{m_b^2}{M_Z^2 - 4m_b^2} \right)$, correspondingly, and can be neglected. The analytical expressions for these contributions can be found in (B1) and (B2) of Appendix.

The QCD one loop contributions to the amplitudes of the discussed processes have exactly

the same Lorentz structure as the electroweak contributions (11) and (12):

$$\begin{aligned}
\mathcal{A}_{QCD}(e^+e^- \rightarrow J/\psi \eta_b) &= \frac{\langle O_{J/\psi} \rangle^{1/2} \langle O_{\eta_b} \rangle^{1/2}}{N_c} \times \\
&\times \frac{4C_A C_F}{N_c} \sqrt{\frac{m_c}{m_b}} e^2 g_s^4 \left(c_\gamma J_\mu + c_Z \tilde{J}_\mu \right) \epsilon_\nu^{J/\psi} P_\rho Q_\sigma \varepsilon^{\mu\nu\rho\sigma} \times \\
&\times \left(\frac{4im_b^2 C_0(4m_b^2, m_c^2, 2m_b^2 - m_c^2 + \frac{s}{2}; 0, 0, m_c)}{16m_b^4 - (s - 4m_c^2)^2} + \right. \\
&- \frac{4im_c^2(-4m_b^2 + 4m_c^2 - s) C_0(m_c^2, 2m_b^2 - m_c^2 + \frac{s}{2}, s; m_c, 0, m_c)}{64m_b^6 - 16m_b^4(4m_c^2 + 3s) - 4m_b^2(16m_c^4 + 8m_c^2 s - 3s^2) + (4m_c^2 - s)^3} + \\
&- \frac{\pi(4m_b^2 - 4m_c^2 + 3s)}{64m_b^6 - 16m_b^4(10m_c^2 + s) + 4m_b^2(32m_c^4 - 12m_c^2 s - s^2) - (2m_c^2 - s)(s - 4m_c^2)^2} + \\
&+ \frac{i(4m_b^2 - 4m_c^2 + 3s) \ln\left(\frac{2m_c^2}{4m_b^2 - 4m_c^2 + s}\right)}{64m_b^6 - 16m_b^4(10m_c^2 + s) + 4m_b^2(32m_c^4 - 12m_c^2 s - s^2) - (2m_c^2 - s)(s - 4m_c^2)^2} + \\
&\left. + \frac{4i\sqrt{s(s - 4m_c^2)} \ln\left(\frac{\sqrt{s(s - 4m_c^2)} + 2m_c^2 - s}{2m_c^2}\right)}{-64m_b^6 + 16m_b^4(12m_c^2 + s) + 4m_b^2(-48m_c^4 + 8m_c^2 s + s^2) + (4m_c^2 - s)^3} \right), \quad (15)
\end{aligned}$$

$$\begin{aligned}
\mathcal{A}_{QCD}(e^+e^- \rightarrow \Upsilon \eta_c) &= \frac{\langle O_\Upsilon \rangle^{1/2} \langle O_{\eta_c} \rangle^{1/2}}{N_c} \times \\
&\times \frac{4C_A C_F}{N_c} \sqrt{\frac{m_b}{m_c}} e^2 g_s^4 \left(b_\gamma J_\mu + b_Z \tilde{J}_\mu \right) \epsilon_\nu^\Upsilon P_\rho Q_\sigma \varepsilon^{\mu\nu\rho\sigma} \times \\
&\times \left(\frac{4im_c^2 C_0(m_b^2, 4m_c^2, -m_b^2 + 2m_c^2 + \frac{s}{2}; m_b, 0, 0)}{16m_b^4 - 8m_b^2 s - 16m_c^4 + s^2} + \right. \\
&+ \frac{4im_b^2(4m_b^2 - 4m_c^2 - s) C_0(m_b^2, -m_b^2 + 2m_c^2 + \frac{s}{2}, s; m_b, 0, m_b)}{64m_b^6 - 16m_b^4(4m_c^2 + 3s) - 4m_b^2(16m_c^4 + 8m_c^2 s - 3s^2) + (4m_c^2 - s)^3} + \\
&- \frac{\pi(-4m_b^2 + 4m_c^2 + 3s)}{32m_b^6 - 32m_b^4(4m_c^2 + s) + 2m_b^2(80m_c^4 + 24m_c^2 s + 5s^2) - (s - 4m_c^2)^2(4m_c^2 + s)} + \\
&- \frac{i(4m_b^2 - 4m_c^2 - 3s) \ln\left(\frac{2m_b^2}{4m_c^2 - 4m_b^2 + s}\right)}{32m_b^6 - 32m_b^4(4m_c^2 + s) + 2m_b^2(80m_c^4 + 24m_c^2 s + 5s^2) - (s - 4m_c^2)^2(4m_c^2 + s)} + \\
&- \frac{4i\sqrt{s(s - 4m_b^2)} \ln\left(\frac{\sqrt{s(s - 4m_b^2)} + 2m_b^2 - s}{2m_b^2}\right)}{64m_b^6 - 48m_b^4(4m_c^2 + s) + 4m_b^2(48m_c^4 + 8m_c^2 s + 3s^2) - (s - 4m_c^2)^2(4m_c^2 + s)} \left. \right), \quad (16)
\end{aligned}$$

where C_0 is the scalar three-point Passarino-Veltman function $\text{ScalarC0}[\mathbf{s}_1, \mathbf{s}_{12}, \mathbf{s}_2; \mathbf{m}_0, \mathbf{m}_1, \mathbf{m}_2]$ defined in package X.

As already mentioned the virtual photon does not decay to the $J/\psi\Upsilon$ pair due to the charge parity conservation, while the virtual Z_0 -boson does. The Lorentz structure of this amplitude is a little bit more complicated than presented in (11) and (12), as contains the additional polarization vector and consists of two components:

$$\begin{aligned} \mathcal{A}_{EW}(e^+e^- \rightarrow J/\psi \Upsilon) &= \frac{\langle O_{J/\psi} \rangle^{1/2} \langle O_\Upsilon \rangle^{1/2}}{N_c} \times \\ &\times \frac{e^4 e_b e_c \sqrt{m_b m_c}}{N_c \cos \theta_w \sin \theta_w (s - M_Z^2 + i\Gamma M_Z)} \tilde{J}_\mu \epsilon_{\nu_1}^{J/\psi} \epsilon_{\nu_2}^\Upsilon \varepsilon^{\mu\nu_1\nu_2\sigma} \times \\ &\times \left(\frac{P_\sigma}{m_c^2 (4m_b^2 - 4m_c^2 - s)} - \frac{Q_\sigma}{m_b^2 (4m_b^2 - 4m_c^2 + s)} \right). \end{aligned} \quad (17)$$

The photonic parts of the electroweak amplitudes (11) and (12) turn into each other under simultaneous permutations $m_b \longleftrightarrow m_c$, $e_b \longleftrightarrow e_c$ and $P \longleftrightarrow Q$, as expected. The same applies for the photonic parts of the one loop QCD amplitudes (15) and (16).

It is interesting to note, that EW and QCD amplitudes for the vector-pseudoscalar production have a different asymptotic behaviour:

$$\left. \frac{\mathcal{A}_{QCD}}{\mathcal{A}_{EW}} \right|_{s \rightarrow \infty} \sim \frac{\ln s}{s}. \quad (18)$$

V. CROSS SECTIONS ESTIMATIONS

The numerical values of parameters used in the calculations are presented in Tab. I. The values of NRQCD matrix elements are adopted from the potential model [16]. The strong coupling constant is used within the two loops accuracy:

$$\alpha_S(Q) = \frac{4\pi}{\beta_0 L} \left(1 - \frac{\beta_1 \ln L}{\beta_0^2 L} \right), \quad (19)$$

where $L = \ln Q^2/\Lambda^2$, $\beta_0 = 11 - \frac{2}{3}N_f$ and $\beta_1 = 102 - \frac{38}{3}N_f$ with $N_f = 6$; the reference value is $\alpha_S(M_Z) = 0.1185$. The appropriate scale $Q = \sqrt{s}$ is chosen for α_s in the full range of energies. For sake of simplicity the fine structure constant is used in Thomson limit: $\alpha = 1/137$.

Table I. The parameters used in the calculations. The NRQCD matrix elements are adopted from [16].

$m_c = 1.5 \text{ GeV}$	$m_b = 4.5 \text{ GeV}$	$M_Z = 91.2 \text{ GeV}$	$\Gamma_Z = 2.5 \text{ GeV}$
$\langle O \rangle_{J/\psi} = \langle O \rangle_{\eta_c} = 0.523 \text{ GeV}^3$			
$\langle O \rangle_\Upsilon = \langle O \rangle_{\eta_b} = 2.797 \text{ GeV}^3$			
$\sin^2 \theta_w = 0.23$			

The cross sections reference values are given in Table II. In the Figures 2 to 5 the calculated cross sections and there ratios are performed as functions of \sqrt{s} .

In the Figure 2 we compare the QCD and EW contributions at low energies (left) and at energies around a Z_0 -mass (right). In the Figure 3 the total cross sections including all discussed contributions are demonstrated. In the Figure 4 the ratios between QCD and EW contributions are performed. The relative contribution of Z_0 -boson annihilation to the studied processes is shown in Figure 5.

Table II. The cross section values in fb at different collision energies. $\sigma(\sqrt{s}_{max})$ is the value in the peak near the threshold.

	\sqrt{s}_{max}	$\sqrt{s} = 20 \text{ GeV}$	$\sqrt{s} = 0.25M_Z$	$\sqrt{s} = 0.5M_Z$	$\sqrt{s} = M_Z$	$\sqrt{s} = 2M_Z$
$J/\psi \eta_b$	$7.20 \cdot 10^{-5}$	$4.22 \cdot 10^{-5}$	$2.53 \cdot 10^{-5}$	$9.85 \cdot 10^{-7}$	$2.29 \cdot 10^{-5}$	$4.14 \cdot 10^{-9}$
$\Upsilon \eta_c$	$1.06 \cdot 10^{-3}$	$1.67 \cdot 10^{-4}$	$6.79 \cdot 10^{-7}$	$8.08 \cdot 10^{-7}$	$2.40 \cdot 10^{-6}$	$1.04 \cdot 10^{-9}$
$J/\psi \Upsilon$	—	$3.82 \cdot 10^{-8}$	$4.07 \cdot 10^{-8}$	$6.52 \cdot 10^{-8}$	$4.98 \cdot 10^{-5}$	$4.17 \cdot 10^{-9}$

As it can be concluded from the presented Figures 2 to 5, the QCD and EW subprocesses contribute differently to the total yield of $J/\psi \eta_b$ and $\Upsilon \eta_c$. In the $J/\psi \eta_b$ production the QCD and EW contributions are comparable at low energies, while the EW contribution dominates around Z_0 pole. Contrary, in the $\Upsilon \eta_c$ production the QCD and EW contributions are comparable at energies around Z_0 pole, while at low energies the QCD contribution dominates.

As can be seen in the Figure 3, both the $J/\psi \eta_b$ -pair and the $\Upsilon \eta_c$ -pair production cross sections have a maximum near the threshold ($\sqrt{s}_{max}(J/\psi \eta_b) \approx 15.6 \text{ GeV}$ and $\sqrt{s}_{max}(\Upsilon \eta_c) \approx 14.1 \text{ GeV}$). The cross section ratios near the maximum take the following values:

$$\frac{\sigma_{QCD}(J/\psi \eta_b)}{\sigma_{EW}(J/\psi \eta_b)} \sim 2, \quad \frac{\sigma_{QCD}(\Upsilon \eta_c)}{\sigma_{EW}(\Upsilon \eta_c)} \sim 10^3, \quad \frac{\sigma_{tot}(\Upsilon \eta_c)}{\sigma_{tot}(J/\psi \eta_b)} \sim 15. \quad (20)$$

As already mentioned, near the Z_0 pole the discussed cross sections behave completely differently:

$$\frac{\sigma_{QCD}(J/\psi \eta_b)}{\sigma_{EW}(J/\psi \eta_b)} \sim 10^{-3}, \quad \frac{\sigma_{QCD}(\Upsilon \eta_c)}{\sigma_{EW}(\Upsilon \eta_c)} \sim 1, \quad \frac{\sigma_{tot}(\Upsilon \eta_c)}{\sigma_{tot}(J/\psi \eta_b)} \sim 10^{-1}. \quad (21)$$

It can be concluded from Equation (18) that the one loop QCD contribution should decrease with energy faster than the EW one. Indeed, as shown in the Figure 4 starting approximately

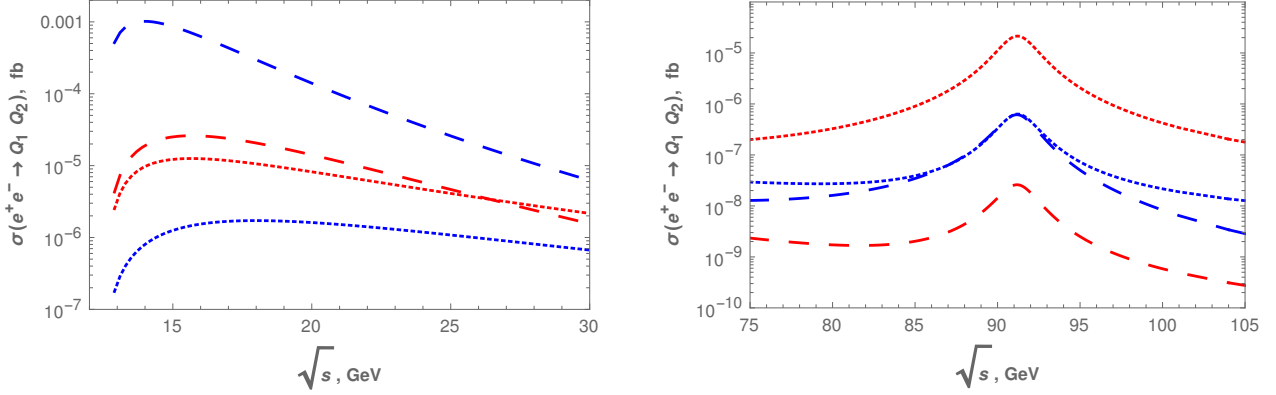


Figure 2. The EW and QCD contributions to the cross sections at low energies (left) and around Z_0 pole (right): the QCD one loop contribution to $\sigma(J/\psi \eta_b)$ (red dashed curve); the EW contribution to $\sigma(J/\psi \eta_b)$ (red dotted curve); the QCD one loop contribution to $\sigma(\Upsilon \eta_c)$ (blue dashed curve); the EW contribution to $\sigma(\Upsilon \eta_c)$ (blue dotted curve).

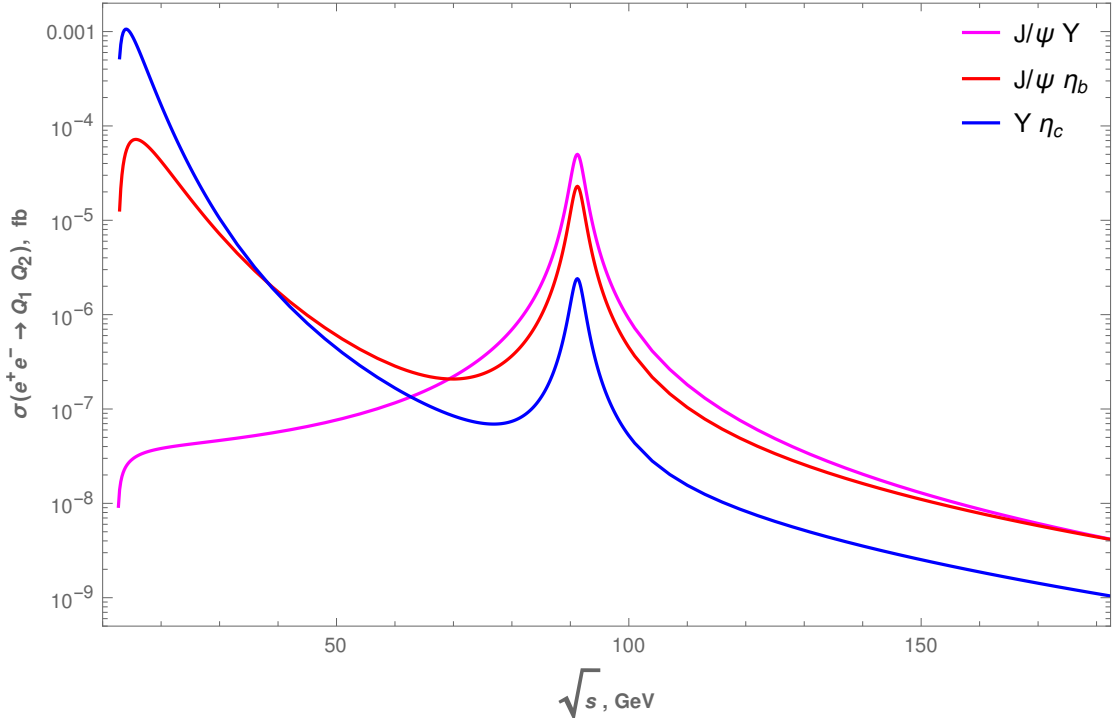


Figure 3. The total cross sections dependence on the collision energy.

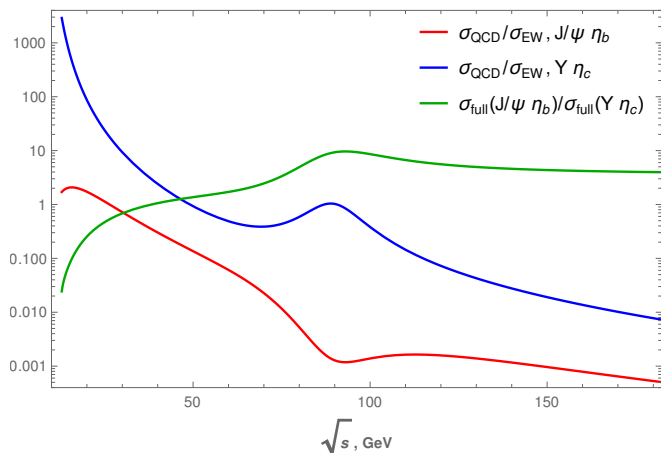


Figure 4. The cross section ratios as a function of the collision energy: $\sigma_{QCD}(J/\psi \eta_b)/\sigma_{EW}(J/\psi \eta_b)$ (red curve), $\sigma_{QCD}(\Upsilon \eta_c)/\sigma_{EW}(\Upsilon \eta_c)$ (blue curve), $\sigma_{tot}(J/\psi \eta_b)/\sigma_{tot}(\Upsilon \eta_c)$ (green curve).

from energies 30 GeV for the $J/\psi \eta_b$ -pair production and from 50 GeV for the $\Upsilon \eta_c$ -pair production the EW contribution exceeds the QCD contribution.

As can be seen from the Figure 3, the single boson production of $J/\psi \Upsilon$ pair is extremely suppressed at low energies against the VP-pair production. However at energies higher than 70 GeV the production cross section of $J/\psi \Upsilon$ pair becomes greater than the other cross sections: $\sigma(J/\psi \Upsilon) > \sigma(J/\psi \eta_b) > \sigma(\Upsilon \eta_c)$. For example, for the chosen parameter values at $\sqrt{s} = M_Z$ we obtain that

$$\sigma(J/\psi \Upsilon) : \sigma(J/\psi \eta_b) : \sigma(\Upsilon \eta_c) = 20.8 : 9.5 : 1. \quad (22)$$

The Z_0 boson exchange obviously dominates at Z_0 pole, however it is also essentially contributes to the production cross section in the wide range around this pole. The energy

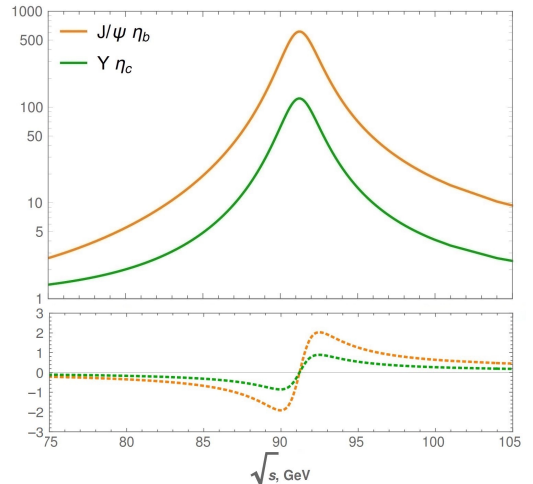


Figure 5. The Z_0 -boson relative contributions as a function of energy: $\sigma_{\gamma+Z_0}(J/\psi \eta_b)/\sigma_{\gamma}(J/\psi \eta_b)$ (solid orange curve) and $\sigma_{\gamma+Z_0}(\Upsilon \eta_c)/\sigma_{\gamma}(\Upsilon \eta_c)$ (solid green curve), as well as the relative contributions of the interference term between γ and Z_0 : $\sigma_{\gamma Z_0}^{int}(J/\psi \eta_b)/\sigma_{\gamma}(J/\psi \eta_b)$ (dashed orange curve) and $\sigma_{\gamma Z_0}^{int}(\Upsilon \eta_c)/\sigma_{\gamma}(\Upsilon \eta_c)$ (dashed green curve).

range where the contribution of Z_0 exchange to the total cross sections is greater than 20% is $E > 60$ GeV for the J/ψ η_b -pair production and $70 \text{ GeV} < E < 150$ GeV for the Υ η_c -pair production. These intervals are asymmetrical with the Z_0 -boson mass due to the interference term (see the bottom plot in the Figure 5).

VI. CONCLUSIONS

The exclusive production of the charmonium-bottomonium pairs ($J/\psi\eta_b$, $\Upsilon\eta_c$, and $J/\psi\Upsilon$) has been studied in single boson e^+e^- annihilation in the energy range from the threshold to $\sqrt{s} = 2M_Z$ within the color singlet approximation of NRQCD.

Both J/ψ η_b and Υ η_c productions essentially differ from the thoroughly investigated J/ψ η_c production, because the main QCD contribution to these processes contains loops and occurs comparable in magnitude with the purely electromagnetic contribution ($\mathcal{O}(\alpha_{em}^2\alpha_s^4)$ v.s. $\mathcal{O}(\alpha_{em}^4)$). This is why the QCD contribution, the electromagnetic contribution and their interference have been studied together. As concerned the J/ψ Υ -pair production, in the leading order this process goes through the electroweak Z_0 boson exchange only. The rather simple structure of the studied amplitudes allows to provide the analytical expressions right in the paper.

In the current study we have shown, that the QCD and EW subprocesses contribute differently to the total yield of J/ψ η_b and Υ η_c . In the J/ψ η_b production the QCD and EW contributions are comparable at low energies, while the EW one highly dominates around Z_0 pole. Contrary, in the Υ η_c production the QCD contribution highly dominates at low energies, while at energies around Z_0 pole the QCD and EW contributions are comparable.

We also have demonstrated that the one-loop QCD amplitude and the electroweak amplitude have different asymptotic behavior at high energies: $\mathcal{A}_{QCD}/\mathcal{A}_{EW}\Big|_{s\rightarrow\infty} \sim \ln s/s$.

The energy sufficient to produce a charmonium-bottomonium pair can not be achieved at the current e^+e^- experiments. Nevertheless we believe that the obtained results may be of considerable interest for experiments at future e^+e^- colliders.

Authors would like to thank A. Likhoded, A. Onishchenko and S. Poslavsky for help and fruitful discussions. The work was supported by foundation RFBR, grant # 20-02-00154 A. I. Belov acknowledges the support from ‘‘BASIS’’ Foundation, grant # 20-2-2-2-1.

REFERENCES

- [1] E. Braaten and J. Lee, Phys. Rev. D **67**, 054007 (2003), [Erratum: Phys.Rev.D 72, 099901 (2005)], arXiv:hep-ph/0211085.
- [2] K. Abe *et al.* (Belle), Phys. Rev. D **70**, 071102 (2004), arXiv:hep-ex/0407009.
- [3] B. Aubert *et al.* (BaBar), Phys. Rev. D **72**, 031101 (2005), arXiv:hep-ex/0506062.
- [4] H.-R. Dong, F. Feng, and Y. Jia, Phys. Rev. D **85**, 114018 (2012), arXiv:1204.4128 [hep-ph]; X.-H. Li and J.-X. Wang, Chin. Phys. C **38**, 043101 (2014), arXiv:1301.0376 [hep-ph]; F. Feng, Y. Jia, and W.-L. Sang, (2019), arXiv:1901.08447 [hep-ph]; Y.-J. Zhang, Y.-j. Gao, and K.-T. Chao, Phys. Rev. Lett. **96**, 092001 (2006), arXiv:hep-ph/0506076; B. Gong and J.-X. Wang, Phys. Rev. D **77**, 054028 (2008), arXiv:0712.4220 [hep-ph]; A. Bondar and V. Chernyak, Phys. Lett. B **612**, 215 (2005), arXiv:hep-ph/0412335; V. Braguta, A. Likhoded, and A. Luchinsky, Phys. Rev. D **72**, 074019 (2005), arXiv:hep-ph/0507275; A. Berezhnoy and A. Likhoded, Phys. Atom. Nucl. **70**, 478 (2007), arXiv:hep-ph/0602041; V. Braguta, A. Likhoded, and A. Luchinsky, Phys. Lett. B **635**, 299 (2006), arXiv:hep-ph/0602047; G. T. Bodwin, D. Kang, and J. Lee, Phys. Rev. D **74**, 114028 (2006), arXiv:hep-ph/0603185; D. Ebert and A. Martynenko, Phys. Rev. D **74**, 054008 (2006), arXiv:hep-ph/0605230; A. Berezhnoy, Phys. Atom. Nucl. **71**, 1803 (2008); D. Ebert, R. Faustov, V. Galkin, and A. Martynenko, Phys. Lett. B **672**, 264 (2009), arXiv:0803.2124 [hep-ph]; V. Braguta, A. Likhoded, and A. Luchinsky, Phys. Rev. D **78**, 074032 (2008), arXiv:0808.2118 [hep-ph]; V. Braguta, Phys. Rev. D **79**, 074018 (2009), arXiv:0811.2640 [hep-ph]; Y.-J. Sun, X.-G. Wu, F. Zuo, and T. Huang, Eur. Phys. J. C **67**, 117 (2010), arXiv:0911.0963 [hep-ph]; V. Braguta, A. Likhoded, and A. Luchinsky, Phys. Atom. Nucl. **75**, 97 (2012); Z. Sun, X.-G. Wu, Y. Ma, and S. J. Brodsky, Phys. Rev. D **98**, 094001 (2018), arXiv:1807.04503 [hep-ph].
- [5] R. Aaij *et al.* (LHCb), Sci. Bull. **65**, 1983 (2020), arXiv:2006.16957 [hep-ex].
- [6] M. Koratzinos (FCC-ee study), Nucl. Part. Phys. Proc. **273-275**, 2326 (2016), arXiv:1411.2819 [physics.acc-ph].
- [7] K. Desch *et al.* (KEK International Working Group), (2019).
- [8] K. Long, D. Lucchesi, M. Palmer, N. Pastrone, D. Schulte, and V. Shiltsev, Nature Phys. **17**,

- 289 (2021), arXiv:2007.15684 [physics.acc-ph].
- [9] A. M. Sirunyan *et al.* (CMS), Phys. Lett. B **797**, 134811 (2019), arXiv:1905.10408 [hep-ex].
- [10] A. Berezhnoy, A. Likhoded, A. Onishchenko, and S. Poslavsky, Nucl. Phys. B **915**, 224 (2017), arXiv:1610.00354 [hep-ph].
- [11] A. V. Berezhnoy, I. N. Belov, S. V. Poslavsky, and A. K. Likhoded, (2021), arXiv:2101.01477 [hep-ph].
- [12] Z.-Q. Chen, H. Yang, and C.-F. Qiao, Phys. Rev. D **102**, 016011 (2020), arXiv:2005.07317 [hep-ph].
- [13] G. T. Bodwin, E. Braaten, and G. P. Lepage, Phys. Rev. D **51**, 1125 (1995), [Erratum: Phys.Rev.D 55, 5853 (1997)], arXiv:hep-ph/9407339.
- [14] G. T. Bodwin, H. S. Chung, D. Kang, J. Lee, and C. Yu, Phys. Rev. D **77**, 094017 (2008), arXiv:0710.0994 [hep-ph].
- [15] H. S. Chung, J. Lee, and C. Yu, Phys. Lett. B **697**, 48 (2011), arXiv:1011.1554 [hep-ph].
- [16] E. J. Eichten and C. Quigg, (2019), arXiv:1904.11542 [hep-ph].
- [17] T. Hahn, Comput. Phys. Commun. **140**, 418 (2001), arXiv:hep-ph/0012260.
- [18] V. Shtabovenko, R. Mertig, and F. Orellana, Comput. Phys. Commun. **256**, 107478 (2020), arXiv:2001.04407 [hep-ph].
- [19] F. Feng, Comput. Phys. Commun. **183**, 2158 (2012), arXiv:1204.2314 [hep-ph].
- [20] A. Smirnov, JHEP **10**, 107 (2008), arXiv:0807.3243 [hep-ph].
- [21] H. H. Patel, Comput. Phys. Commun. **218**, 66 (2017), arXiv:1612.00009 [hep-ph].
- [22] S. Laporta, Int. J. Mod. Phys. A **15**, 5087 (2000), arXiv:hep-ph/0102033.

Appendix A: $\langle O \rangle$ and $|R(0)|^2$ values

Table A.I. $\langle O \rangle$ and $|R(0)|^2$ (where possible) in GeV^3 for J/ψ , η_c , Υ and η_b mesons.

Ref.	$\langle O \rangle_{J/\psi}/ R_{J/\psi}(0) ^2$	$\langle O \rangle_{\eta_c}/ R_{\eta_c}(0) ^2$	$\langle O \rangle_{\Upsilon}/ R_{\Upsilon}(0) ^2$	$\langle O \rangle_{\eta_b}/ R_{\eta_b}(0) ^2$
[1]	0.335 ± 0.024	0.297 ± 0.032		
[14]	$0.440^{+0.067}_{-0.055}$	$0.434^{+0.169}_{-0.158}$		
[16]	0.523/1.0952		2.797/5.8588	
[15]			$3.069^{+0.207}_{-0.190}$	

Appendix B: Electroweak amplitudes with $\mathcal{O}\left(\frac{m_q^2}{M_Z^2 - 4m_q^2}\right)$ corrections

$$\begin{aligned} \mathcal{A}_{EW}(e^+e^- \rightarrow J/\psi \eta_b) &= \frac{\langle O_{J/\psi} \rangle^{1/2} \langle O_{\eta_b} \rangle^{1/2}}{N_c} \times \\ &\times \frac{-e^4 e_b e_c}{2N_c m_c \sqrt{m_b m_c} (s + 4m_c^2 - 4m_b^2)} \left(b_\gamma (1 + A_1) J_\mu + b_Z (1 + A_2) \tilde{J}_\mu \right) \epsilon_\nu^{J/\psi} P_\rho Q_\sigma \epsilon^{\mu\nu\rho\sigma}. \quad (\text{B1}) \end{aligned}$$

$$\begin{aligned} \mathcal{A}_{EW}(e^+e^- \rightarrow \Upsilon \eta_c) &= \frac{\langle O_\Upsilon \rangle^{1/2} \langle O_{\eta_c} \rangle^{1/2}}{N_c} \times \\ &\times \frac{e^4 e_b e_c}{2N_c m_b \sqrt{m_b m_c} (s + 4m_b^2 - 4m_c^2)} \left(c_\gamma (1 + A_3) J_\mu + c_Z (1 + A_4) \tilde{J}_\mu \right) \epsilon_\nu^\Upsilon P_\rho Q_\sigma \epsilon^{\mu\nu\rho\sigma}. \quad (\text{B2}) \end{aligned}$$

$$\begin{aligned} \mathcal{A}_{EW}(e^+e^- \rightarrow J/\psi \Upsilon) &= \frac{\langle O_{J/\psi} \rangle^{1/2} \langle O_\Upsilon \rangle^{1/2}}{N_c} \times \\ &\times \frac{e^4 e_b e_c \sqrt{m_b m_c}}{N_c \cos \theta_w \sin \theta_w (s - M_Z^2 + i\Gamma M_Z)} \tilde{J}_\mu \epsilon_{\nu_1}^{J/\psi} \epsilon_{\nu_2}^\Upsilon \epsilon^{\mu\nu_1\nu_2\sigma} \times \\ &\times \left(\frac{P_\sigma}{m_c^2 (4m_b^2 - 4m_c^2 - s)} (1 + A_5) - \frac{Q_\sigma}{m_b^2 (4m_b^2 - 4m_c^2 + s)} (1 + A_6) \right). \quad (\text{B3}) \end{aligned}$$

$$\begin{aligned}
A_1 &= - \left(\frac{m_c^2}{M_Z^2 - 4m_c^2} \right) \frac{(4e_b \sin^2 \theta_w + 1) (4e_c \sin^2 \theta_w - 1)}{4e_b e_c \cos^2 \theta_w \sin^2 \theta_w}, \\
A_2 &= - \left(\frac{m_c^2}{M_Z^2 - 4m_c^2} \right) \frac{(4e_c \sin^2 \theta_w - 1) \left((4m_b^2 - 4m_c^2) (4e_b \sin^2 \theta_w + 1)^2 + s (8e_b \sin^2 \theta_w (2e_b \sin^2 \theta_w + 1) + 3) \right)}{4e_b e_c \cos^2 \theta_w \sin^2 \theta_w (4e_b \sin^2 \theta_w + 1) (4m_b^2 - 4m_c^2 + s)}, \\
A_3 &= - \left(\frac{m_b^2}{M_Z^2 - 4m_b^2} \right) \frac{(4e_b \sin^2 \theta_w + 1) (4e_c \sin^2 \theta_w - 1)}{4e_b e_c \cos^2 \theta_w \sin^2 \theta_w}, \\
A_4 &= - \left(\frac{m_b^2}{M_Z^2 - 4m_b^2} \right) \frac{(4e_b \sin^2 \theta_w + 1) \left((4m_b^2 - 4m_c^2) (4e_c \sin^2 \theta_w - 1)^2 - s (8e_c \sin^2 \theta_w (2e_c \sin^2 \theta_w - 1) + 3) \right)}{4e_b e_c \cos^2 \theta_w \sin^2 \theta_w (4e_c \sin^2 \theta_w - 1) (4m_b^2 - 4m_c^2 - s)}, \\
A_5 &= - \left(\frac{m_c^2}{M_Z^2 - 4m_c^2} \right) \frac{(4e_b \sin^2 \theta_w + 1) (4e_c \sin^2 \theta_w - 1) (4m_b^2 - 4m_c^2 + 3s)}{4e_b e_c \cos^2 \theta_w \sin^2 \theta_w (4m_b^2 - 4m_c^2 + s)}, \\
A_6 &= - \left(\frac{m_b^2}{M_Z^2 - 4m_b^2} \right) \frac{(4e_b \sin^2 \theta_w + 1) (4e_c \sin^2 \theta_w - 1) (4m_b^2 - 4m_c^2 - 3s)}{4e_b e_c \cos^2 \theta_w \sin^2 \theta_w (4m_b^2 - 4m_c^2 - s)}.
\end{aligned}$$

Appendix C: The electromagnetic production cross section of VP pair

The electromagnetic contribution σ_{QED} (diagrams of type (a), intermediate photons only) is given by the formula:

$$\sigma_{QED} = \frac{32\pi^3 \alpha^4 e_b^4 e_c^2 \mathcal{O}_{\eta_b} \mathcal{O}_{J/\psi} \left(16m_b^4 - 8m_b^2 (4m_c^2 + s) + (s - 4m_c^2)^2 \right)^{3/2}}{3m_b m_c^3 N_c^4 s^3 (-4m_b^2 + 4m_c^2 + s)^2}, \quad (C1)$$

where the $\Upsilon \eta_c$ case follows under $(m_b \longleftrightarrow m_c, e_b \longleftrightarrow e_c)$ permutation.